Available online at www.sciencedirect.com

ScienceDirect

Ceramics International 40 (2014) 7219–7225

CERAMICS INTERNATIONAL

www.elsevier.com/locate/ceramint

A facile synthesis of reduced graphene oxide-wrapped WO_3 nanowire composite and its enhanced electrochemical catalysis properties

Meng Huang[a,b], Yan Wu[b], Weibing Hu[a,*]

[a]Key Laboratory of Biological Resources Protection and Utilization of Hubei Province, Hubei Minzu University, Enshi 445000, PR China
[b]Department of Chemistry, Hubei Minzu University, Enshi 445000, PR China

Received 20 November 2013; received in revised form 15 December 2013; accepted 15 December 2013
Available online 21 December 2013

Abstract

Uniform reduced graphene oxide-wrapped WO_3 nanowire nanocomposite (RGO–WO_3 nanowire) was prepared by a one-step solvothermal method. The resulting RGO–WO_3 nanowire was first characterized by using FT-IR, XRD, AFM and SEM, and then was used to modify the glassy carbon electrode (GCE). The electrochemical behavior of honokiol on the unmodified GCE, WO_3 nanowire modified GCE and RGO–WO_3 nanowire modified GCE was compared. The RGO–WO_3 nanowire composite has remarkably enhanced the electrochemical character of honokiol, with a significantly improved current value of oxidation peak in the composite modified GCE. After 2-min under open circuit, a linear range from 1.0×10^{-8} to 2.0×10^{-5} mol/L and detection limit of honokiol as low as 8×10^{-9} mol/L were obtained. This analysis method has a high recovery ratio of honokiol up to 103%.

Keywords: B. Nanocomposites; Electrochemical detection; Honokiol; Reduced graphene oxide; WO_3 nanowire

1. Introduction

Graphene, a two dimensional monolayer of sp^2 carbon in a honeycomb-like network [1], has attracted a great deal of scientific interest due to its outstanding mechanical, electrical, thermal, and optical properties [2]. It is considered as a promising material in various applications such as transparent conducting films [3], sensors [4], supercapacitors [5], and batteries [6]. As a consequence, significant efforts have been devoted to utilizing graphene as a 2D support to anchor nanoparticles, including Fe_3O_4 [7], TiO_2 [8], SnO_2 [9], MnO_2 [10], CdSe [11], $Co(OH)_2$ [12], $Ni(OH)_2$ [13] and WO_3 [14]. In general, such graphene-based nanocomposites are prepared from the reduction of graphene oxide (GO)-based nanocomposites through a chemical method or heat treatment. However, these methods generally suffer from some harsh conditions, such as the use of organic solvents, poisonous agents, and heat treatment processes. Particularly, the reducing agent hydrazine with a strong alkalescency may lead to the destruction of hybrid nanocomposites by the excess OH^- ions. In addition, the hydrothermal wrapping oxide nanomaterials have been the subject of intensive research because of their remarkable electronic, mechanical, and thermal properties. Graphene-wrapped TiO_2 nanoparticles were prepared by a two-step hydrothermal process and calcinations [15], exhibiting excellent photocatalytic property under visible light for the degradation of methylene blue with a rate constant of 3.41×10^{-2} min^{-1}.

Honokiol is an effective component of the bark of *Magnolia officinalis* which is a drug regularly prescribed in traditional Chinese medicine. Honokiol has been reported to show many pharmacological activities, including antimicrobial, antiplatelet, antioxidant, and anti-inflammatory [16–18]. Therefore, it is quite important and interesting to develop simple and sensitive methods for determining honokiol. Recently, direct electrochemical detection of honokiol has attracted increasing attention since the electroanalytical method exhibits many advantages, such as high sensitivity, short analysis time, low cost and convenient handling. For example, a mesoporous silica modified

*Corresponding author. Tel.: +86 718 8439811; fax: +86 718 8437422.
E-mail address: chemistryhu@126.com (W. Hu).

0272-8842/$ - see front matter © 2013 Elsevier Ltd and Techna Group S.r.l. All rights reserved.
http://dx.doi.org/10.1016/j.ceramint.2013.12.061

carbon paste electrode (CPE) was successfully used to detect honokiol [19]. Mesoporous materials with unique structure and extraordinary properties can greatly improve the sensitivity of electrochemical detection [20,21]. Compared with the unmodified CPE, the mesoporous silica modified CPE enhanced the oxidation peak current and the detection sensitivity of honokiol. The limit of detection was 1.8×10^{-9} mol/L and the analysis time was about 3 min. Besides, a glassy carbon electrode coated with acetylene black nanoparticle was also reported for the detection of honokiol [22], which achieved a limit of detection of 1.88×10^{-8} mol/L. In our previous work [23], the WO_3 modified carbon paste electrode achieved a honokiol detection linear range between 3×10^{-8} and 2.0×10^{-5} mol/L, and a detection limit of 1×10^{-8} mol/L after 2-min accumulation. However, to the best of our knowledge, electrochemical determination of honokiol using the RGO–WO_3 nanowire composite materials modified electrode has not been reported. In this research, we use a quick and simple method to synthesize the RGO–WO_3 nanowire composite materials by a one-step method.

2. Experimental

2.1. Preparation of graphite oxide

Graphite oxide (GO) is obtained by chemical oxidation from graphite [8]. Graphite, $KMnO_4$, sulfuric acid (98%) and a Teflon reactor were completely cooled in a refrigerator at 0–4 °C before use. The Teflon reactor (100 mL) was placed in a stainless steel autoclave. The cooled graphite (0.5 g) and $KMnO_4$ (3 g) were put into the reactor, and then sulfuric acid (50 mL) was added. As soon as the sulfuric acid was added, the reactor and stainless steel autoclave were covered and fastened down. The autoclave was kept at 0–4 °C for 1.5 h and then heated at 100 °C in an oven for 1.5 h. The obtained mud was diluted with 100 ml distilled water. With mechanical stirring, H_2O_2 (30%) was dripped into the suspension until the slurry turned golden yellow. The suspension was washed with hot 0.2 M HCl and deionized water until the pH reached 7. Finally, the clean suspension was dried at 60 °C, to obtain the dark brown solid of graphite oxide.

2.2. Synthesis of WO_3 nanowire, RGO and RGO–WO_3 nanowire composite materials

GO was dispersed in ethanol, subjected to ultrasonic treatment for 1.5 h, and then the suspension was filtered. A stable solution of GO was obtained, and its concentration was 0.5 mg/mL (30 mL weight of 15 mg). 30 mL of GO ethanol solution was added to the 100 mL Teflon container. 25 mg of WCl_6 (99.99%) was slowly dissolved in 50 mL ethanol to obtain a uniform solution, which was then transferred to the above 100 mL Teflon container. After sealing, the Teflon-lined stainless steel pressure vessel was heated at 180 °C for 16 h. Using the same method, WO_3 nanowires [24] were also obtained without GO ethanol solution; RGO [25] was obtained without using WCl_6 ethanol solution. After reaction, the product was centrifuged, washed with distilled water and acetone each three times, and then dried at 60 °C.

2.3. Preparation of RGO–WO_3 nanowire, WO_3 nanowire and RGO modified GCE

GCE (3 mm in diameter) was first polished with 1.0, 0.3 and 0.05 μm alumina powders, rinsed thoroughly with distilled water, and then sonicated in a 1:1 nitric acid solution, ethanol and distilled water and allowed to dry at room temperature. 10-mg RGO–WO_3 nanowire, WO_3 nanowire, and RGO were sonicated in 10 mL distilled water to obtain a stable suspension. An aliquot of 10 μL of RGO–WO_3 nanowire, or WO_3 nanowire or RGO was then dropped onto the surface of the GCE. Followed by drying at the room temperature, the modified GCEs (RGO–WO_3 nanowire/GCE, WO_3 nanowire/GCE and RGO/GCE) were finally obtained.

2.4. Characterization

Atomic force microscope (AFM) images of GO were recorded with a multimode scanning probe microscope (CSPM-5500, Beijing, China). Particle size and morphology of the powders were examined with a SEM (JSM-6510LV, Japan). The structure of products was characterized by XRD (Shimadzu XRD-7000, Japan) using Cu-Kα radiation (γ for Kα=is 1.54 Å) at 40 kV and 40 mA. Infrared spectra of products were recorded on a Nicolet 360 FT-IR instrument using a KBr pellet in the 400–4000 cm^{-1} range.

All the electrochemical measurements were performed using a 660D electrochemical analyzer (CH Instruments, USA). A conventional three-electrode system, consisting of RGO–WO_3 composites modified working GCEs, a saturated calomel reference electrode (SCE) and a platinum wire auxiliary electrode, was employed. Otherwise, 0.1 M, pH 6.5 phosphate buffer saline (PBS) solution was used as the supporting electrolyte for the detection of honokiol. Cyclic voltammetry (CV) tests were conducted at a scan rate of 100 mV s^{-1} from 0 to 1.0 V. Differential pulse voltammetry (DPV) was used to study the electrochemical behavior in low concentrations of honokiol from 0.15 to 0.75 V. The electrochemical reaction mechanism was studied at different scan rates using linear sweep voltammetry (LSV).

3. Results and discussion

Fig. 1 shows the AFM picture of GO. The flakes of GO are presented in Fig. 1a, which show a thickness of about 1.24 nm (Fig. 1b). Considering the impact noise of instrument, we believe that the actual GO thickness should be about 1.0 nm, which is consistent with the literature [26].

SEM observation results of the materials are presented in Fig. 2. WO_3 nanowires (Fig. 2a) of about 21 nm in diameter are shown. Fig. 2b shows the nanosheet morphology of RGO with seriously folded edges. At a low magnification (Fig. 3c), the RGO is found to be well-expanded with the fabrication of

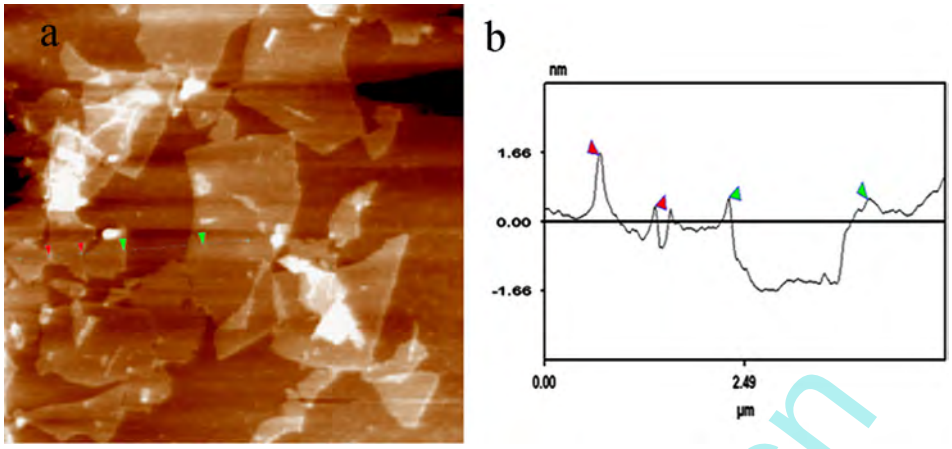

Fig. 1. AFM picture of GO.

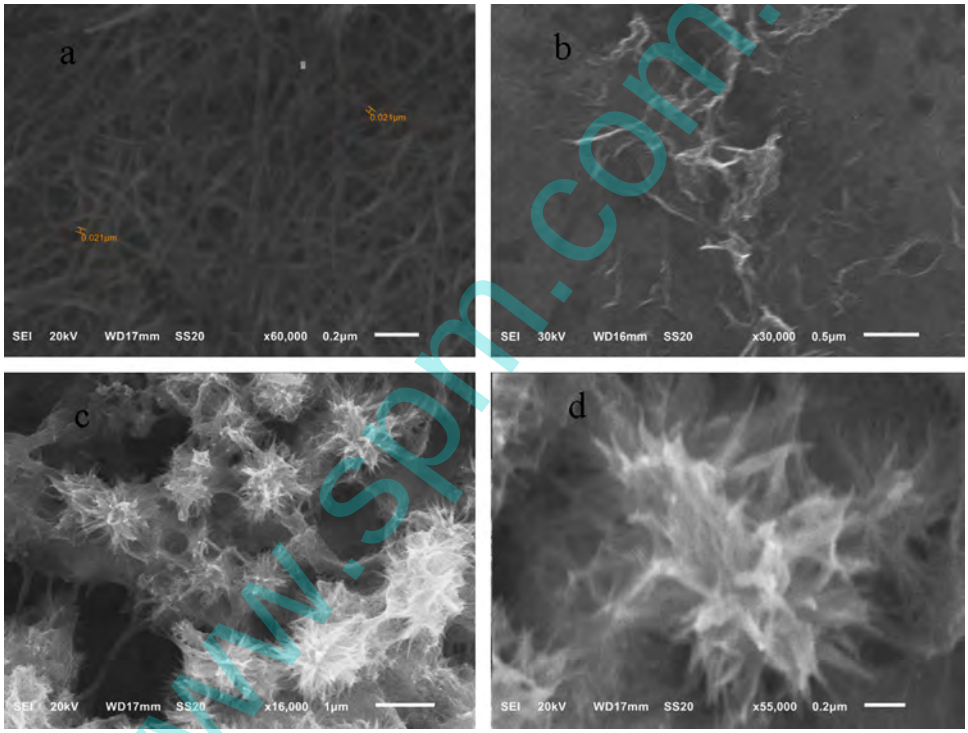

Fig. 2. SEM observations of the materials: (a) WO_3 nanowires, (b) RGO, (c) a low magnification SEM image exhibiting general morphology of the RGO–WO_3 nanowire composite, and (d) a higher magnification SEM image with reduced graphene oxide-wrapped WO_3 nanowire composite.

WO_3 nanowires. The nanowires were wrapped by the RGO nanosheets (Fig. 3d).

GO, RGO, WO_3 nanowire and RGO–WO_3 nanowire are further characterized by infrared spectroscopy (FT-IR) as shown in Fig. 3. C–O functional groups such as COOH (1724 cm^{-1}), C–OH (1045 cm^{-1}) and the stretching peak of the C–OH group (3428 cm^{-1}) are clearly visible in GO. The spectrum also shows a C=C peak at 1635 cm^{-1} corresponding to the remaining sp^2. From the picture, GO obtained was well-reduced compared to the profile of RGO. The interaction between the WO_3 and RGO–WO_3 nanowires was also confirmed by FT-IR spectroscopy. The partial absorption bands between 1300 and 4000 cm^{-1} are mainly assigned to the chemisorbed and/or physisorbed H_2O and CO_2 molecules on the surface of the nanostructured WO_3 crystals. The broad absorptions at low frequencies were ascribed to the vibration of W–O–W bond [14] (below 1000 cm^{-1}) which was not observed in the spectrum of GO and RGO.

Fig. 4 shows the XRD patterns of the as-prepared RGO–WO_3 nanocomposite and RGO. As shown in Fig. 4(a), all the peaks can be indexed to the hexagonal phase of WO_3 (JCPDS no. 75-2187). One typical diffraction peak (002) of RGO is also presented in Fig. 4(a), which is consistent with the XRD pattern of bare RGO shown in Fig. 4(b).

Based on the above results, a possible growth mechanism of RGO–WO_3 nanowire nanocomposite is illustrated in Scheme 1. First, a large amount of WO_x was formed in the ethanol steam. Second, the WO_x was transformed into WO_3 crystal nucleus

around the surface of GO. As known, GO sheet has its basal planes decorated mostly with epoxy and hydroxyl groups, while carbonyl and carboxyl groups are located at the edges. Thus, those functional groups, acting as anchor sites, enabled the subsequent in situ formation of small WO_3 nanowires on the surface [27]. And the nanowires were wrapped by the graphene oxide nanosheets through hydrogen-bond interaction of the oxygen-containing functional groups. At the same time, solvothermal reduction at high temperature was reported to be an effective route to restore the sp^2-hybridized network. As a result, GO was simultaneously reduced to graphene, accompanied by the growth of WO_3 nanowire on the 2-D carbon support during the hydrothermal reaction.

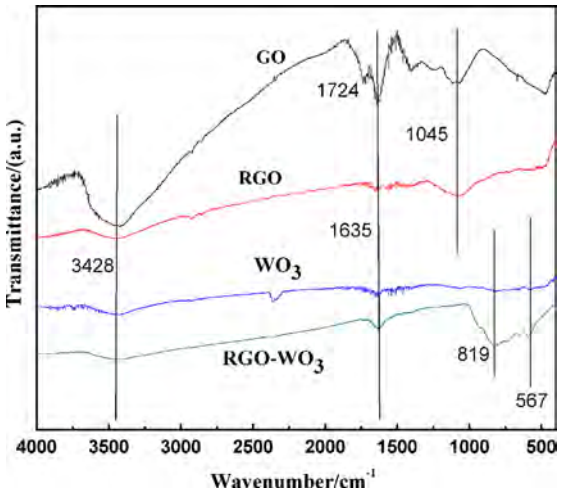

Fig. 3. FT-IR spectra of GO, RGO, WO_3 nanowire and RGO–WO_3 nanowire.

The electrochemical responses of honokiol on the surface of GCE, WO_3 nanowire, RGO and RGO–WO_3 nanowire modified GCE were studied using cyclic voltammetry (CV). Fig. 5 shows the CV curves of 5 μM honokiol in a pH 6.5 PBS solution. Because the RGO of this method modified GCE did not responded to the honokiol, it is not shown in the CV curves. After 2 min under open circuit, the first anodic sweep from 0.0 to 1.0 V, an oxidation peak was observed at 0.47 V on the GCE surface (curve b). On the reverse potential scan from 1 V to 0.0 V, a very small reduction peak appeared at 0.42 V. The peak potential separation was about 50 mV on the surface of GCE. Likewise, a wide oxidation peak was observed at 0.52 V on the WO_3 modified GCE surface (curve b), and a weak reduction peak appeared at 0.40 V. The peak potential separation was about 120 mV on the surface of WO_3 nanowire modified GCE. However, the electrochemical behavior of honokiol showed great difference on the RGO–WO_3 nanowire modified GCE surface (curve a). First, the peak currents were all greatly increased. Second, the peak potential separation decreased to 26 mV. According to Nicholson′s theory [28,29], a smaller peak potential separation reveals a better reversibility and higher heterogeneous electron exchange rate. Furthermore, the peak current of honokiol greatly decreased on the second

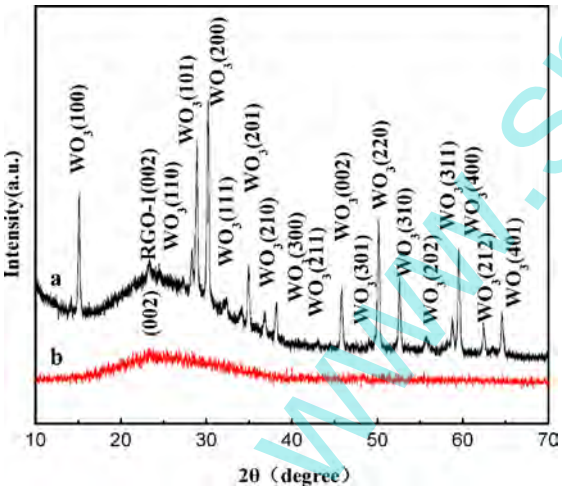

Fig. 4. Line a is the XRD profile of RGO–WO_3 composite material, and line b is the XRD profile of reduced graphene oxide.

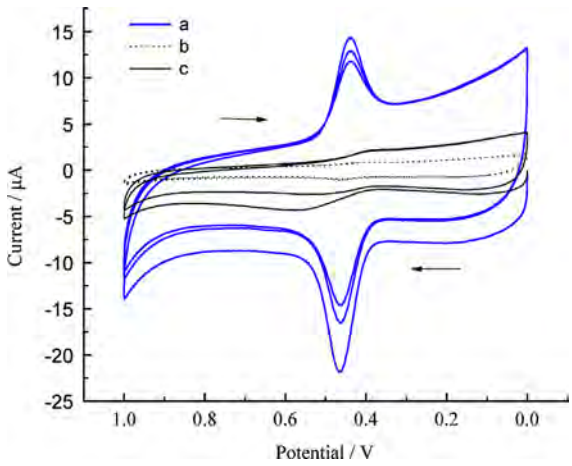

Fig. 5. CV curves of 5 μM honokiol on RGO–WO_3 nanowire modified GCE (a), GCE (b) and WO_3 nanowire modified GCE (c) in pH 6.5 PBS solution. Scan rate: 100 mV s^{-1}.

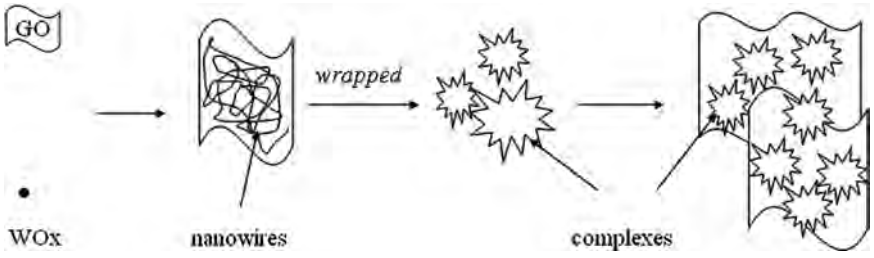

Scheme 1. The possible growth mechanism of RGO–WO_3 nanowire nanocomposite.

anodic sweep. This may be caused by the fact that the reaction product of honokiol is adsorbed on the electrode surface, decreasing the electrode activity. Hence, to achieve high sensitivity and good reproducibility, the peak current in the first sweep was chosen for the analysis of honokiol.

In order to further demonstrate the prominent influence of RGO–WO_3 nanowire modified GCE in the detection of honokiol, differential pulse voltammetry (DPV) was used to study the electrochemical behavior in low concentration honokiol. Fig. 6 indicates the DPV curves of 2 μM honokiol on GCE and RGO–WO_3 nanowire modified GCE. After 2-min accumulation under open circuit, an oxidation peak at 0.42 V was observed on the unmodified GCE surface (curve a). However, the oxidation peak current of honokiol was significantly improved on the surface of RGO–WO_3 modified GCE under the identical conditions (curve c). In contrast, the DPV curve of RGO–WO_3 nanowire modified GCE in the absence of honokiol is also given (curve b). The peak current enhancement reveals that RGO–WO_3 nanowire has remarkably increased the sensitivity of detection of honokiol. The excellent conductivity, catalytic performance, and the large specific surface areas of RGO–WO_3 exhibited a strong adsorptive ability, and provided numerous active sites for honokiol. Therefore, the oxidation peak current of honokiol was greatly enhanced. By contrast, curve b is featureless, indicating that the oxidation peak is attributed to honokiol. Finally, curves b and c were not as smooth as curve a, which may be due to the fact that RGO–WO_3 nanowire composite has far more numerous active sites than those of the others.

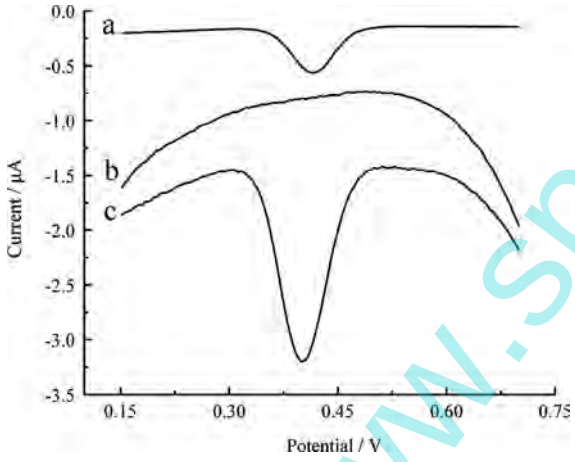

Fig. 6. DPV curves of 2 μM honokiol on GCE (a), RGO–WO_3 nanowire modified GCE (c) in pH 6.5 PBS solution, and RGO–WO_3 nanowire modified GCE (b) in pH 6.5 PBS solution without honokiol.

The electrochemical response of 5 μM honokiol at different scan rates was studied using linear sweep voltammetry (LSV), to help discuss the electrochemical reaction mechanism [30]. In this process, two noticeable characteristics were discovered. First, with the increase of the scanning speed, the oxidation peak current increases and the reduction peak potential gradually decreases; the differences between oxidation and reduction peaks become larger. Second, the ratio of the absolute value of reduction peak current to oxidation peak current approximately equals 1 at smaller scanning speed, but less than 1 and even smaller at increased scanning speed. Thus, (1) the reaction process is irreversible; (2) the reaction is reactant adsorption process, that is $A \leftrightarrow Aads + ne^- \rightarrow B$; and (3) because the oxidation peak potential is proportional to ln (V), a linear relationship is $Ep = 0.36654 + 0.01543 \ln V$, the correlation coefficient is 0.992, and the slope is $RT/\alpha nF$ ($\alpha = 0.5$), so four electrons are involved in the electrochemical reaction of honokiol.

The electrochemical behavior of honokiol in different supporting electrolytes was discussed by cyclic voltammetry, including phosphate buffer solution, Tris buffer solution, Hac–NaAc, B–R buffer solution, PBS, HCl and $HClO_4$ solution (concentration is 0.1 mol/L). From comparison, it was found that the peak current of honokiol was more sensitive in PBS solution. Hence, the relationship between pH value and oxidation peak potential (E_{pa}) of honokiol was evaluated using PBS solution. It was found that the E_{pa} shifted linearly to more negative potentials along with increasing pH value from 5.7 to 8.0. The linear regression equation is $E_{pa}/V = 0.65978 - 0.03038$pH, and the correlation coefficient is 0.998. The slope is $2.303RT/\alpha nF$. Hence, four protons were involved in the reaction of honokiol. The most sensitive response signal was obtained when the pH value of supporting electrolyte was controlled at 6.5 under the condition of a minimum value of base current. Finally, the above analysis

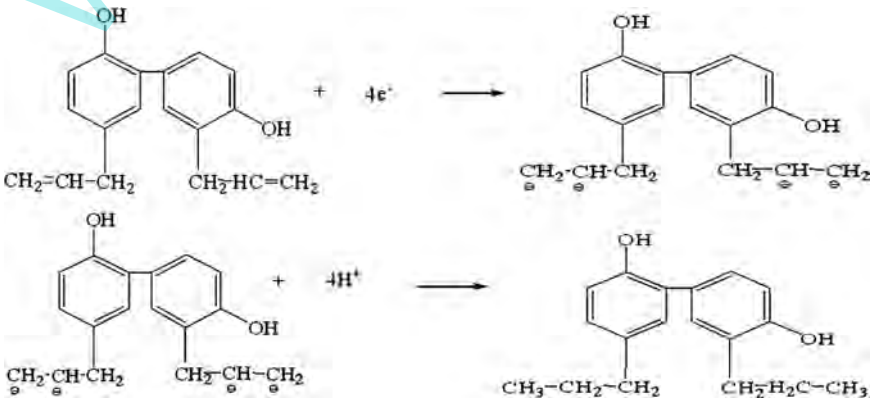

Fig. 7. The electrochemical reaction mechanism of honokiol.

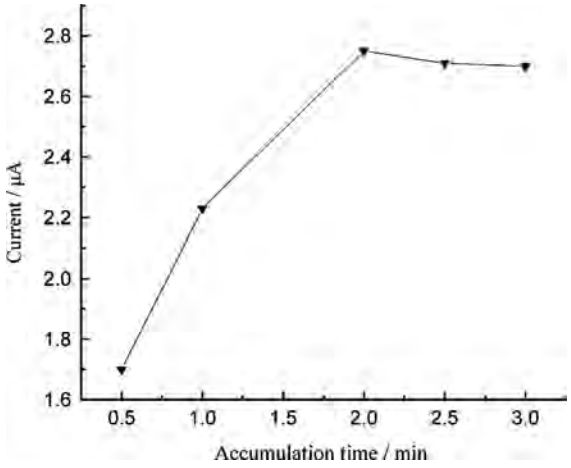

Fig. 8. Influence of accumulation time on the oxidation peak current of 8 μM honokiol.

suggests that the numbers of transferred proton and electron are equal. In accordance with the literature [31], the possible reaction mechanism is surmised in Fig. 7.

The effect of accumulation time on the oxidation peak current of honokiol was evaluated using DPV. In this process, we have found that the accumulation potential has no obvious influence on the oxidation peak current of honokiol; therefore the accumulation was carried out under open circuit. Fig. 8 depicts the relationship between the oxidation peak current of 8 μM honokiol and accumulation time. At an accumulation time between 0 and 2 min, the oxidation peak current of honokiol was greatly increased, indicating that accumulation obviously improved the determining sensitivity. When further improving the accumulation time from 2 to 3 min, the oxidation peak current decreased slightly; hence a 2-min accumulation time was used.

The RGO–WO_3 modified GCE was used for single determination in this work. The reproducibility for multiple modified GCEs was estimated by measuring the peak current of 2 μM honokiol. In order to obtain good reproducibility, each freshly modified electrode needs to be swept in the PBS solution until background current is at the minimum and stabilized. The relative standard deviation (RSD) is 6.6% for five RGO–WO_3 modified GCEs, indicating a good reproducibility.

Under the optimal conditions, the oxidation peak current of honokiol (I_A, μA) was linear with its concentration (C_A, μM) in the range of 1×10^{-8}–2×10^{-5} mol/L, obeying the following equation: $I_A(\mu A) = -0.1812C_A\,(\mu M) - 1.16549$. The correlation coefficient was 0.998, suggesting a good linearity. After 2 min accumulation under open circuit, the limit of detection was evaluated to be 8.0×10^{-9} mol/L, based on three signal to noise ratios.

The potential interferences of some foreign species on the determination of honokiol were also examined. There was no influence on the determination of 2 μM honokiol when 500-fold concentration of common ions (Cu^{2+}, Fe^{3+}, Mg^{2+}, Zn^{2+}, and Pb^{2+}), or 100-fold of pyrogallol, resorcinol and 2-nitrophenol were added to the electrolytic cell. Though there was a wide interference peak in voltage of 0.55 V when 10-fold concentration of honokiol was added, it had no interference in the determination. The peak current values of honokiol change were below 5.2%.

Table 1
Determination recovery of honokiol.

Found before adding (mol/L)	Added (mol/L)	Found after adding (mol/L)	Recovery (%)	RSD (%) $n=5$
1.00×10^{-6}	0.00	1.10×10^{-6}	110	4.1
	1.00×10^{-6}	1.95×10^{-6}	97.7	3.2
	1.50×10^{-6}	2.56×10^{-6}	102.4	5.4

Under the optimized conditions, honokiol in actual water was determined using a standard addition method and each concentration was continuously measured five times. Table 1 shows the results of recycling experiment. These results showed clearly that the recovery was between 97.7% and 110%. The correlation coefficient was under 6%.

4. Conclusion

RGO–WO_3 nanowire composite materials were synthesized using a facile solvothermal method, and formed uniform coating of WO_3 nanowires on the RGO sheets. The glassy carbon electrode modified by the resulting RGO–WO_3 nanowire composite has been successfully used to measure honokiol content by the electrochemical method. The composites possess increased surface area with more reaction site for interaction, which results in a significantly improved current value of oxidation peaks for honokiol. The use of RGO–WO_3 nanowire modified electrode can reliably and effectively determine the low honokiol concentration of 1.0×10^{-8} mol/L, with a detection limitation as low as 8×10^{-9} mol/L.

Acknowledgment

This work was supported by Open Foundation of Key Laboratory of Biologic Resources Protection and Utilization of Hubei Province, Forestry Key Disciplines (No. PKLHB1303), the National Natural Science Foundation of China (No. 20871044) and Hubei Minzu University (MY2009B007).

References

[1] A.K. Geim, K.S. Novoselov, The rise of graphene, Nat. Mater. 7 (2007) 6183–6191.
[2] K.S. Novoselov, A.K. Geim, S.V. Morozov, D. Jiang, M.I. Katsnelson, I.V. Grigorieva, S.V. Dubonos, A.A. Firsov, Two-dimensional gas massless Dirac fermions in graphene, Nature 438 (2005) 197–200.
[3] Jonathan K. Wassei, Richard B. Kaner, Graphene, a promising transparent conductor, Mater. Today 13 (2010) 52–59.
[4] Z.G. Cheng, Q. Li, Z.J. Li, Q.Y. Zhou, Y. Fang, Suspended graphene sensors with improved signal and reduced noise, Nano Lett. 10 (2010) 1864–1868.
[5] H.L. Wang, Q.l. Hao, X.J. Yang, L.D. Lu, X. Wan, Graphene oxide doped polyaniline for supercapacitors, Electrochem. Commun. 11 (2009) 1158–1161.

[6] C.Y. Wang, D. Li, C.O. Too, Electrochemical properties of graphene paper electrodes used in lithium batteries, Chem. Mater. 21 (2009) 2604–2606.
[7] W.J. Li, Z.K. Tan, T.R. Kuykendall, S. Aloni, S.D. Xun, E. Lin, V. Battaglia, Y.G. Zhang, Fe_3O_4 nanoparticle-integrated graphene sheets for high-performance half and full lithium ion cells, Phys. Chem. Chem. Phys. 13 (2011) 7170–7177.
[8] D.H. Wang, D.W. Choi, J. Li, Z.G. Yang, Z.M. Nie, R. Kou, D.H. Hu, C.M. Wang, L.V. Saraf, J.G. Zhang, I.A. Aksay, J. Liu, Self-assembled TiO_2–graphene hybrid nanostructures for enhanced Li-ion insertion, ACS Nano 3 (2009) 907–914.
[9] L.S. Zhang, L.Y. Jiang, H.Y. Yan, W. Wang, W.W. Song, Y.G. Guo, L.J. Wan, Mono dispersed SnO_2 nanoparticles on both sides of single layer graphene sheets as anode materials in Li-ion batteries, J. Mater. Chem. 20 (2010) 5462–5467.
[10] Z.S. Wu, W.C. Ren, D.W. Wang, F. Li, B.L. Liu, H.M. Cheng, High-energy MnO_2 nanowire/graphene and graphene asymmetric electrochemical capacitors, ACS Nano 4 (2010) 5835–5842.
[11] Y. Lin, K. Zhang, W.F. Chen, Y.D. Liu, Z.G. Geng, J. Zeng, N. Pan, L.F. Yan, X.P. Wang, J.G. Hou, Dramatically enhanced photo response of reduced graphene oxide with linker-free anchored CdSe nanoparticles, ACS Nano 4 (2010) 3033–3038.
[12] S. Chen, J.W. Zhu, X. Wang, One-step synthesis of graphene–cobalt hydroxide nanocomposites and their electrochemical properties, J. Phys. Chem. C 114 (2010) 11829–11834.
[13] H.L. Wang, H.S. Casalongue, Y.Y. Liang, H.J. Dai, $Ni(OH)_2$ nanoplates grown on graphene as advanced electrochemical pseudocapacitor materials, J. Am. Chem. Soc. 132 (2010) 7472–7477.
[14] J.J. Guo, Y. Li, S.M. Zhu, Z.X. Chen, Q.L. Liu, D. Zhang, W.J. Moon, D.M. Song, Synthesis of WO_3@Graphene composite for enhanced photocatalytic oxygen evolution from water, RSC Adv. 2 (2012) 1356–1363.
[15] J.S. Lee, K.H. You, C.B. Park, Highly photoactive, low bandgap TiO_2 nanoparticles wrapped by graphene, Adv. Mater. 24 (2012) 1084–1088.
[16] M. Ogata, M. Hoshi, K. Shimotohno, S. Urano, T. Endo, Antioxidant activity of magnolol, honokiol, and related phenolic compounds, J. Am. Oil Chem. Soc. 74 (1997) 557–562.
[17] J. Park, J. Lee, E. Jung, Y. Park, K. Kim, B. Park, K. Jung, E. Park, J. Kim, D. Park, In vitro antibacterial and anti-inflammatory effects of honokiol and magnolol against *Propionibacterium* sp, Eur. J. Pharmacol. 496 (2004) 189–195.
[18] Y.R. Lin, H.H. Chen, C.H. Ko, M.H. Chan, Neuroprotective activity of honokiol and magnolol in cerebellar granule cell damage, Eur. J. Pharmacol. 537 (2006) 64–69.
[19] J. Zhao, W.S. Huang, X.J. Zheng, Mesoporous silica-based electrochemical sensor for simultaneous determination of honokiol and magnolol, J. Appl. Electrochem. 39 (2009) 2415–2419.
[20] F.R. Wang, J.Q. Yang, K.B. Wu, Mesoporous silica-based electrochemical sensor for sensitive determination of environmental hormone bisphenol A, Anal. Chim. Acta 638 (2009) 23–28.
[21] H.G. Lin, X.B. Ji, Q.Y. Chen, Y.K. Zhou, C.E. Banks, K.B. Wu, Mesoporous-TiO_2 nanoparticles based carbon paste electrodes exhibit enhanced electrochemical sensitivity for phenols, Electrochem. Commun. 11 (2009) 1990–1995.
[22] X.F. Yang, M.M. Gao, H.D. Hu, H.J. Zhang, Phytochem. Anal. 22 (2011) 291.
[23] W.Y. Qu, X.Y. Xiong, W.B. Hu, P. Zhang, Q. Luo, S.H. Zhang, Surface enhancement of WO_3 nanowires toward the oxidation and electrochemical detection of honokiol in traditional Chinese medicine, Colloid Surf. B 100 (2012) 103–106.
[24] C. Nethravathi, M. Rajamathi, Chemically modified graphene sheets produced by the solvothermal reduction of colloidal dispersions of graphite oxide, Carbon 46 (2008) 1994–1998.
[25] W.B. Hu, Y.I. Zhao, Z.L. Liu, C.W. Dunnill, D.H. Gregory, Y.Q. Zhu, Nanostructural evolution: from one-dimensional tungsten oxide nanowires to three-dimensional ferberite flowers, Chem. Mater. 20 (2008) 5657–5665.
[26] V.H. Pham, T.V. Cuong, S.H. Hur, E. Oh, E.J. Kim, E.W. Shin, J.S. Chung, Chemical functionalization of graphene sheets by solvothermal reduction of a graphene oxide suspension in N-methyl-2-pyrrolidone, J. Mater. Chem. 21 (2011) 3371–3377.
[27] X.Q. An, J.C. Yu, Y. Wang, Y.M. Hu, X.L. Yu, G.G. Zhang, WO_3 nanorods/graphene nanocomposites for high-efficiency visible-light-driven photocatalysis and NO_2 gas sensing, J. Mater. Chem. 22 (2012) 8525–8531.
[28] R.S. Nicholson, Theory of stationary electrode polarography single scan and cyclic methods applied to reversible, irreversible, and kinetic systems, Anal. Chem. 36 (1964) 706–723.
[29] R.S. Nicholson, Theory and application of cyclic voltammetry for measurement of electrode reaction kinetics, Anal. Chem. 37 (1965) 1351–1355.
[30] E. Laviron, General expression of the linear potential sweep voltammogram in the case of diffusionless electrochemical systems, J. Electroanal. Chem. Interfacial Electrochem. 101 (1979) 19–28.
[31] J.B. Hu, S.Y. Gong, C.K. Sun, Z.H. Li, Q.L. Li, Electrochemical behavior and the reaction mechanism of honokiol, Chin. J. Anal. Chem. 5 (2000) 539–543.